

Study of Alkali (Na,K)-Doped $\text{Cu}_2\text{ZnSnS}_4$ Thin Films Prepared by Sol–Gel Method

R. Hosseinpour^a, M. Izadifard^{a,*}, and M. E. Ghazi^a

^a Faculty of Physics, Shahrood University of Technology, Shahrood, Iran

*e-mail: mizadifard@shahroodut.ac.ir

Received September 21, 2020; revised September 21, 2020; accepted October 7, 2020

Abstract—The non-doped and alkali (Na,K)-doped $\text{Cu}_2\text{ZnSnS}_4$ (CZTS) thin films were prepared using the sol–gel spin-coating method on the glass substrate, and the changes in the structural, optical, and electrical characteristics of the films were examined and compared. The structural study results obtained showed that all the prepared samples had a kesterite structure. The scanning electron microscopy and Raman analysis showed that the samples' surface and crystalline quality were significantly changed by doping, and an appropriate amount of dopants can improve them. The optical study showed that the energy gap values for the CZTS layers were in the range of 1.40–1.61 eV, which is desirable for solar cells. Moreover, good optical conductivity values (10^{12} – 10^{15} s^{-1}) and high absorption coefficients (up to 1.8×10^5 cm^{-1} in the visible region) were obtained for the CZTS thin films. Investigation of the sample's electrical properties indicated that non-doped and doped CZTS was *p*-type, and therefore doping did not change the type of the carrier of thin films. Moreover, the carrier concentration of the samples significantly increased up to 8.00×10^{19} cm^{-3} (one order of magnitude increase) with the doping. The samples' photovoltaic properties showed that the fabricated ZnS/CZTS hetero-junction exhibited good rectifying behavior and the doped layers had better diode parameters. Overall, the results showed that the CZTS thin films doped with an appropriate amount of dopants (1% Na and 1.5% K) had better structural, optical, and electrical properties. The photo-electrical study of the samples showed that for all samples, photocurrent under illumination significantly increased (especially for Na-doped CZTS thin films), indicating that the CZTS thin films are suitable for solar energy conversion.

Keywords: sol–gel, $\text{Cu}_2\text{ZnSnS}_4$ (CZTS) thin films, alkali dopants, photodiodes, solar cell

DOI: 10.1134/S1063782621020135

1. INTRODUCTION

$\text{Cu}_2\text{ZnSnS}_4$ (CZTS) is a direct band gap (~ 1.5 eV) semiconductor. This system has attracted much attention as an absorber layer in solar cells because of its advantages, such as a suitable band gap, a high absorption coefficient ($> 10^4$ cm^{-1}) in the range of the visible spectrum [1], and presence of cheap and non-toxic elements in its structure. Thus it can be an appropriate candidate to substitute IGS thin films composed of toxic and expensive materials. Nowadays, the efficiency of the CZTS thin films based on solar cells reaches 12.7% [2], which is lower than the reported 20.3% efficiency of the CIGS-based solar cells [3] and 17.3% efficiency of the CdTe-based solar cells [4], although the theoretical limit of Shockley and Queisser for the efficiency of the CZTS solar cells is 32.2% [5]. Therefore, efforts have been made to increase the open-circuit voltage and the CZTS solar cells' fill factor. The electrical properties of solar cells can be improved by enhancing the absorber layer's charge carrier transport. One way to do so is to add a suitable dopant to the light absorber layer. The potassium and sodium dopants' impact on the characteris-

tics of the CuInGaSe_2 (CIGS) thin-film has been checked [6]. It has been found that doping causes the growth of the grains with (112) preferable orientation, and improves the open-circuit voltage V_{oc} and the fill factor (FF). It has been concluded that these can be due to an increase in the *p*-type conductivity and the passivation of compensating defects [7]. Due to the similarity of the structural CZTS and CIGS, the effects of these dopants on CZTS thin films' characteristics are also considered. There is a limited number of publications on the impact of dopants alkaline features CZTS [8–11]. In this work, we changed the characteristics of CZTS thin films by the K and Na dopants. The CZTS thin films can be prepared by various techniques based on vacuumed [12, 13] and non-vacuumed methods [14, 15]. The sol–gel spin-coating is one of the non-vacuumed solution-based methods used for synthesizing the CZTS thin films because of its facilities and excellent control of the stoichiometry of solvent composition, and low cost of thin-film preparation.

Many researchers have reported that in the highly efficient solar cells with non-stoichiometric CZTS,

the Zn-rich and Cu-poor conditions are more desirable because the Cu-poor thin films lead to the formation of Cu vacancies that may enhance the *p*-type conductivity and prevent the formation of impurity phases [16, 17]. Thus, after examining the experimental results in this work, the $\text{Cu}/(\text{Zn} + \text{Sn}) = 0.90$ and $\text{Zn}/\text{Sn} = 1.13$ conditions were selected, and enhancement in the growth condition was studied [18].

2. EXPERIMENTAL

2.1. Sample Preparation

In this work, the K- and Na-doped CZTS thin layers were synthesized by a sol-gel spin-coating method. In order to prepare the sol-gel solutions, the chloride salts of copper ($\text{CuCl}_2 \cdot 2\text{H}_2\text{O}$, 99%, Merck), zinc (ZnCl_2 , 98%, Merck), and tin ($\text{SnCl}_2 \cdot 2\text{H}_2\text{O}$, 98%, Merck) were dissolved in 20 mL of 2-methoxyethanol solution (2-metho, 99%, Merck). For the preparation of the required solution, thiourea ($\text{SC}(\text{NH}_2)_2$, 99%, Merck), as a sulfur source, and monoethanolamine (MEA, 99.5%, Merck), as a stabilizer, was added to the solution. In order to dope K and Na into the CZTS system, KCl (99%, Merck) with K/Cu molar ratios of 0.5, 1, 1.5, and 2%, and NaCl (99%, Merck) with Na/Cu molar ratios of 0.5, 1, 1.5, and 2% were added to the solution. The prepared solution was stirred for 30 min at 45°C until the entire precursor was fully resolved. The glass substrates were cleaned using normal detergent and then rinsed with deionized water. After that, they were washed carefully in an ultrasonic bath with distilled water, ethanol, acetone, and distilled water, respectively. Finally, the substrates were dried with hot air. The metals' molar ratios in the solution for the samples' preparation were set at $\text{Cu}/(\text{Zn}+\text{Sn}) = 0.9$ and $\text{Zn}/\text{Sn} = 1.13$. Each time, 0.3 mL of the precursor solution was poured on the glass substrate, and the spin-coating process was done at a speed of 2000 rpm for 30 s. The prepared CZTS layers were dried at 200°C in the air in an electric oven for 10 min. The spin-coating drying process was repeated six times for each sample to obtain the desired thickness. The thickness of the samples was around 250 nm, which was estimated by the SEM cross-section image. The annealing was performed in Ar gas at 500°C for 40 min with a heating rate of 9°C/min. without any sulfur supplementation.

2.2. Material Characterizations

The samples' structure was investigated using an X-ray diffractometer (CuK_α radiation, $\lambda = 1.5406 \text{ \AA}$, Bruker, AXS). The morphology of the samples was examined by scanning electron microscopy using a SEM (VEGA\\TESCAN-LMU). The optical properties of the prepared samples were studied by a UV-Visible spectrometer (1800 UV-SHIMADZU model). The Raman scattering measurements were done by a

Raman spectrometer (Ava-Raman-PRB-785) with a 785-nm excitation laser at room temperature. For the electrical property investigation, a four-point probe setup (JANDEL model RM3-AR) and a Hall measurement system under a magnetic field of 0.4 T at room temperature were used. To measure the samples' electrical properties, the elements Mo and Au were deposited by a desk magnetron Sputter Coater (DSR1, Nanostructured Coatings Co. (NSC)) as back and front contacts on a glass substrate.

3. RESULTS AND DISCUSSION

3.1. Structural and Morphological Properties

3.1.1. XRD analysis. The XRD patterns for the non-doped and doped CZTS thin films prepared at different K(Na)/Cu molar ratios are shown in Figs. 1a and 1b.

As it can be seen in both series of the diffraction patterns for the K- or Na-doped samples, diffraction peaks forming the (112), (220), and (312) planes are present, which is characteristic of the kesterite crystal structure (JCPDS no. 26-0575). The relative intensity of (112) diffraction peak (especially in 1.5% K- and 1% Na-doped samples) is dominant in all XRD patterns. The XRD pattern for the 0.5% K-doped sample (Fig. 1a) shows a small Cu_{2-x}S , secondary phase, and the patterns for 1, 1.5, and 2% K-doped samples only show the CZTS single phase. In the case of Na-doped samples, the patterns of 0.5 and 1.5% doped samples show the presence of a small Cu_{2-x}S , secondary phase.

The crystalline size of the samples was estimated by the Debye-Scherrer (DS) equation (Eq. (1)) [19] and the Williamson-Hall (W-H) equation (Eq. (2)) [20].

$$D = \frac{k\lambda}{\beta \cos \theta}, \quad (1)$$

$$\beta \cos \theta = k\lambda/D + 4\epsilon \sin \theta, \quad (2)$$

where β is the full width at half-maximum (FWHM) of the X-ray diffraction peak in radians, k is a constant that is taken equal to 0.9, λ is the wavelength of the X-ray, D is the crystallite size, θ is the Bragg's diffraction angle, and ϵ is the micro-strain. XRD patterns of the samples do not show a significant peak shift, but the lines are broadened as a function of the diffraction angle. To separate the sources of diffraction peak broadening (induced by crystalline size or by strain), the W-H plots were drawn and shown in Fig. 2.

The crystallite size and microscopic strain values for the samples are summarized in Tables 1 and 2.

As is seen from Tables 1 and 2, the difference of crystalline sizes obtain from W-H, and DS equations are not much, indicating that the broadening is mostly due to grain size.

According to the W-H plots, the microscopic strain in the films K is compressive (due to the shrink-

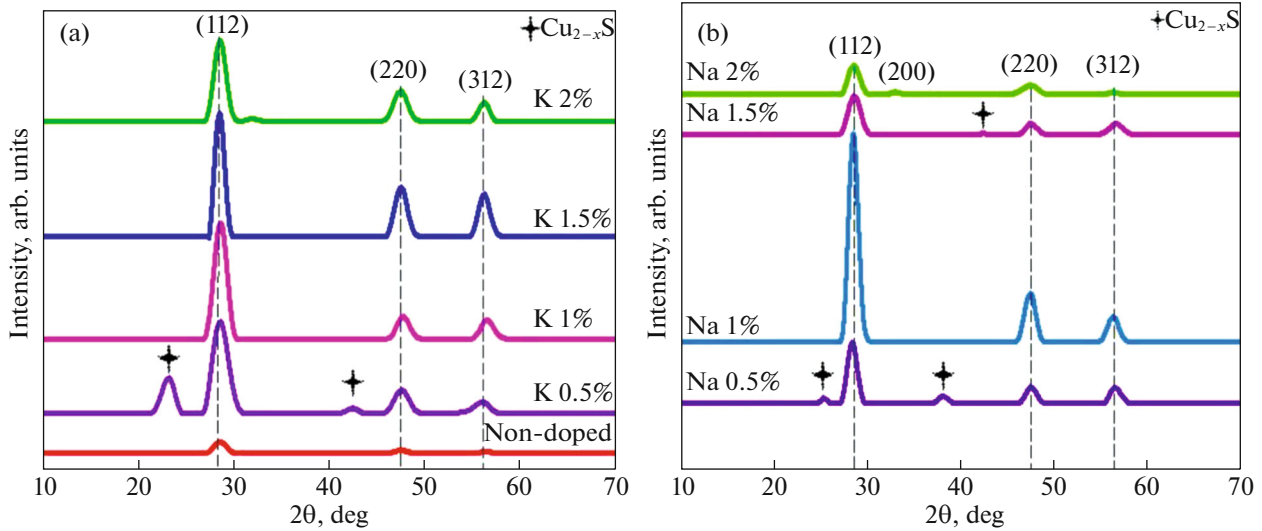


Fig. 1. XRD patterns for (a) K- and (b) Na-doped and non-doped CZTS samples.

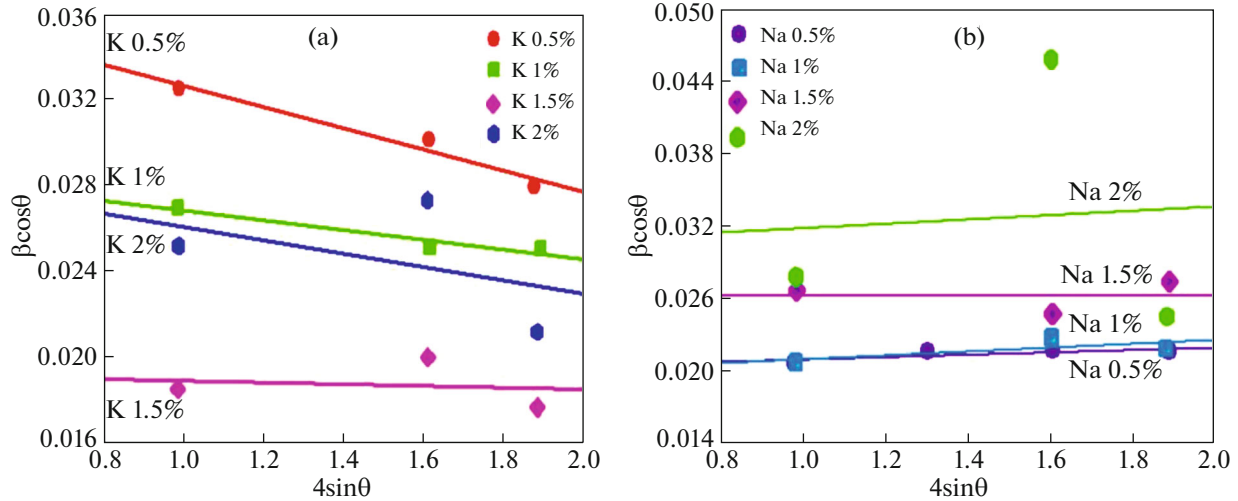


Fig. 2. W–H plots of CZTS thin films doped with different dopant concentrations (a) K and (b) Na.

ing of the unit cell volume), and in the films, Na is tensile (due to the increase of the unit cell volume). The lowest strain values are seen for 1.5% K and 1.5% Na samples. Among the potassium-doped samples, the K (1.5%) sample and the sodium-doped samples, the Na (1%) sample has a larger crystallite size and better crystal structures. As shown in Tables 1 and 2, the samples' crystallite size values are about 5–7 nm. The lattice parameters and cell volumes of the samples were calculated using Eqs. (3)–(5) (using the (112) and (220) diffraction peaks).

$$2d \sin \theta = n\lambda, \tag{3}$$

$$1/d^2 = (h^2 + k^2)/a^2 + l^2/c^2, \tag{4}$$

$$V_{uc} = a^2c, \tag{5}$$

where d is the distance between the planes with indices of hkl , and V_{uc} is the unit cell volume. The results obtained are summarized in Tables 3 and 4.

The CZTS kesterite structure parameters according to the standard card are also reported in this table. According to a computational error reported in this

Table 1. Calculated average crystallite size and micro-strain for K-doped samples

K/Cu ratio, %	0	0.5	1	1.5	2
D_{AV} , nm (DS)	5.27	4.61	5.39	6.16	5.71
D , nm (W–H)	4.93	3.69	4.76	7.30	4.75
ϵ , 10^{-3} (W–H)	–1.18	–4.94	–2.26	–0.368	–3.14

Table 2. Calculated average crystallite size and micro-strain for Na-doped samples

Na/Cu ratio, %	0	0.5	1	1.5	2
D_{Av} , nm (DS)	5.27	6.49	6.39	5.29	5.79
D , nm (W–H)	4.93	6.98	7.17	5.33	4.60
ϵ , 10^{-3} (W–H)	–1.18	1.04	1.62	0.155	1.73

table, the a , b , and c lattice parameters' values agree with the reported kesterite structure's standard lattice parameters within the accuracy indicated in table. The variation in lattice parameters, maybe because of dopant atoms (K, Na) radii is greater than cations atoms radii in CZTS thin films increasing in unit cell volume. This variance of the samples' lattice parameters is also due to the strain distribution variance in the crystal structures. Deviation from the tetragonal structure, $c/2a$, is also shown in Table 3. The $c/2a$ ratio approach to the ideal number of one introduces the formation of the tetragonal crystal structure for the CZTS thin films. The $c/2a$ ratio in the K (1.5%) and Na (1% and 1.5%) samples due to the smaller micro-strains are closer to the ideal number.

3.1.2. Raman analysis. Though the XRD measurements are generally used to identify the phase structure since some of the spectroscopy at room temperature with a 785 nm excitation laser is used to distinguish between these structures. The Raman spectra of the samples are shown in Fig. 3.

In the Raman spectra of all samples, an intense peak around 330 cm^{-1} and two weaker peaks around 283 and 360 cm^{-1} can be seen, which characterize the kesterite CZTS phase [21]. As shown in Fig. 3, the Raman peaks shift toward lower energies compared to the bulk CZTS (336 cm^{-1}), which may be due to the presence of internal stress produced by the shrinking of the unit cell volume [22]; and also there is a small shift of the Raman peaks with doping due to the presence of impurity. In the spectra of the doped samples, there are no obvious characteristic peaks of impurity phases such as Cu_2SnS_3 (303 cm^{-1}) [23], Cu_3SnS_4 (318 cm^{-1}) [24], SnS_2 (314 cm^{-1}) [25], and ZnS (351 cm^{-1}) [26]. Sharper intense peaks in the K (1.5%) and Na (1%) samples indicate better crystalline structures of the kesterite doped CZTS. The Raman spectra

of the samples doped with 2% K and 0.5% Na show a peak at around 475 cm^{-1} , which can be attributed to the Cu_{2-x}S phase [27]. In the other samples, no peak corresponding to the Cu_{2-x}S phase was seen. The results obtained from the Raman spectra are compatible with the XRD patterns and confirmed the formation of the kesterite CZTS thin films. In general, there is no obvious change in Raman peaks positions after doping.

3.1.3. SEM analysis. The morphological structure of the samples was recorded by the SEM images (Figs. 4 and 5).

A comparison between the images shown in Fig. 4 indicates that the non-doped sample's surface has many small grains and some outgrown grains on top of them. In the sample doped with 0.5% of K, a uniform surface is formed, and after 1% K doping, grain growth is observed. However, little cracks were formed, and after increasing the doping concentration up to 1.5%, the grain size increased and wholly covered the substrate, and then it seemed that the grain size began to decrease (2% K sample). In the case of Na-doped samples, shown in Fig. 5, the surfaces are smoother, and in the 1% Na-doped samples, the growth of grains is observed, and in the case of samples doped with 1.5 and 2%, agglomeration and reduction of grain size are seen.

3.2. Optical Properties

The samples' transmission spectra were measured in the range of $300\text{--}1100\text{ nm}$ (Figs. 6a and 6b) to investigate the samples' optical properties.

As Fig. 6a shows, introducing K to the CZTS system increases the transmittance, and the sample doped with 1.5% of K has a higher transmittance than the other samples. The 1.5% doped sample has a bigger grain size, and so has minimum grain boundaries that act as the scattering center. Among the potassium-doped samples, samples doped up to 1.5% showed a higher transmittance than the non-doped samples, consistent with the grain sizes seen in the SEM images. In the case of samples doped with sodium, 1% Na-doped sample has the maximum transmittance, and 2% doped sample has the minimum transmittance; these results agree with the size of the grains found by XRD and SEM.

Table 3. Lattice parameters and unit cell volumes were calculated for samples doped with K and Na

K/Cu ratio, %	0	0.5	1	1.5	2	According to standard card (JCPDS 26-0575)
$a = b$, Å (± 0.002)	5.411	5.405	5.397	5.414	5.414	5.427
c , Å (± 0.002)	10.780	10.752	10.880	10.863	10.759	10.848
$c/2a$	0.996	0.995	1.008	1.002	0.994	0.999
V_{uc} , Å ³	315.63	314.12	316.86	318.37	315.64	319.50

Table 4. Lattice parameters and unit cell volumes were calculated for samples doped with Na

Na/Cu ratio (%)	0	0.5	1	1.5	2	According to standard card (JCPDS 26 -0575)
$a = b, \text{Å} (\pm 0.002)$	5.411	5.411	5.426	5.428	5.425	5.427
$c, \text{Å} (\pm 0.002)$	10.780	11.002	10.868	10.875	10.867	10.848
$c/2a$	0.996	1.017	1.002	1.002	0.991	0.999
$V_{uc}, \text{Å}^3$	315.63	322.10	320.00	320.10	319.82	319.50

Tauc's relation (6) was used [28] to determine the direct optical band gap E_g of the samples.

$$(\alpha hv) = A(hv - E_g)^{1/2}, \quad (6)$$

where h is the Planck's constant, hv is the photons incident's energy, and A is a constant independent from energy. The samples' direct band gaps were determined based on the extrapolated linear regression of the $(\alpha hv)^2$ vs. hv curves. The absorption coefficient α of the samples was calculated according to Eq. (7).

$$\alpha = 1/t \ln[(1 - R)^2/T], \quad (7)$$

R , T , and t are the reflection, transmittance, and thickness of the samples, respectively. The variation in the absorption coefficient with photon energy for the samples is shown in Fig. 7.

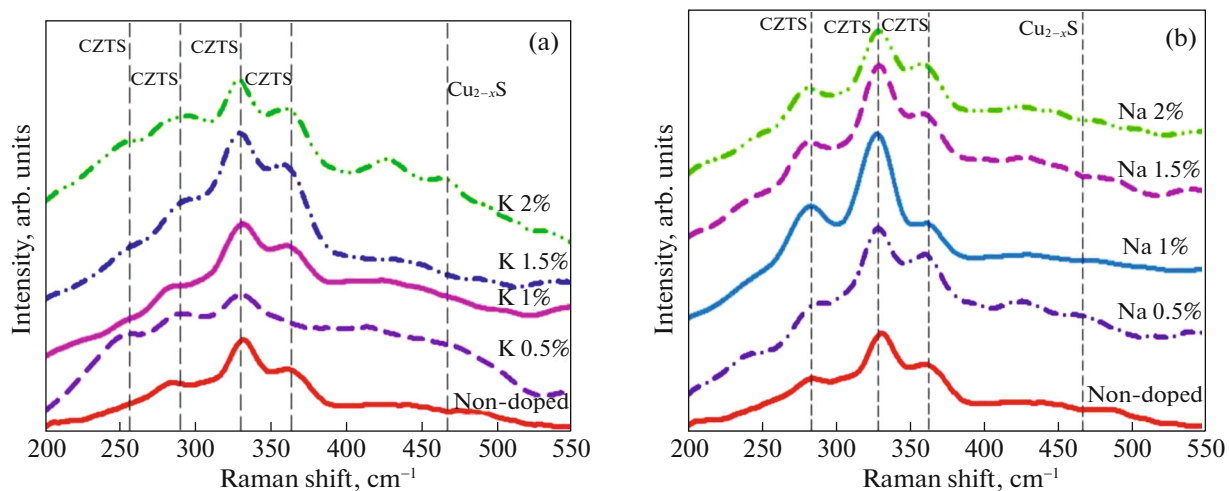
The absorption coefficients of the samples in the visible region are more extensive than 10^4 cm^{-1} . The absorption coefficients for all K sample and Na (0.5, 1.5, 2%) are smaller than a non-doped sample but for 1% Na sample the absorption coefficients is significantly bigger than the non-doped sample. It reaches up to about $1.8 \times 10^5 \text{ cm}^{-1}$ in the visible range, which is an interesting result for the optoelectronic application.

Moreover, Figs. 8a–8c show the $(\alpha hv)^2$ vs. hv curves of the samples plotted to determine the direct band gap energies of the samples.

The calculated direct band gap values for the samples are reported in Table 5.

The optical band gaps obtained are in the range of the values reported for the CZTS thin film [29, 30]. The band gap values are in the range of 1.50–1.59 eV for the K-doped samples and in the range of 1.40–1.61 eV for the Na-doped samples. Therefore, the band gap values have a higher variance for Na-doped samples (about 10%) compared to the band gap of the non-doped sample. In the case of Na-doped samples, reduction in the band gap of K (1.5%) and K (2%) thin films may be due to their larger grain size and occupation of the interstitial site with some of the potassium atoms.

Moreover, band gaps of Na-doped samples decrease after doping, while in the Na (1%), the band gap is increased. Based on the theoretical computational, Zhao et al. have shown that the fundamental absorption edge of Na-doped CZTS has blue-shifted when Na occupies the cation lattice sites, while the fundamental absorption edge is red-shifted when Na occupies the interstitial site [31]. An increase in the band gap of Na (1%) can be due to Na's substitution with Cu atoms. In sum up, the potassium and sodium

**Fig. 3.** Raman spectra of doped-CZTS films with (a) K and (b) Na.

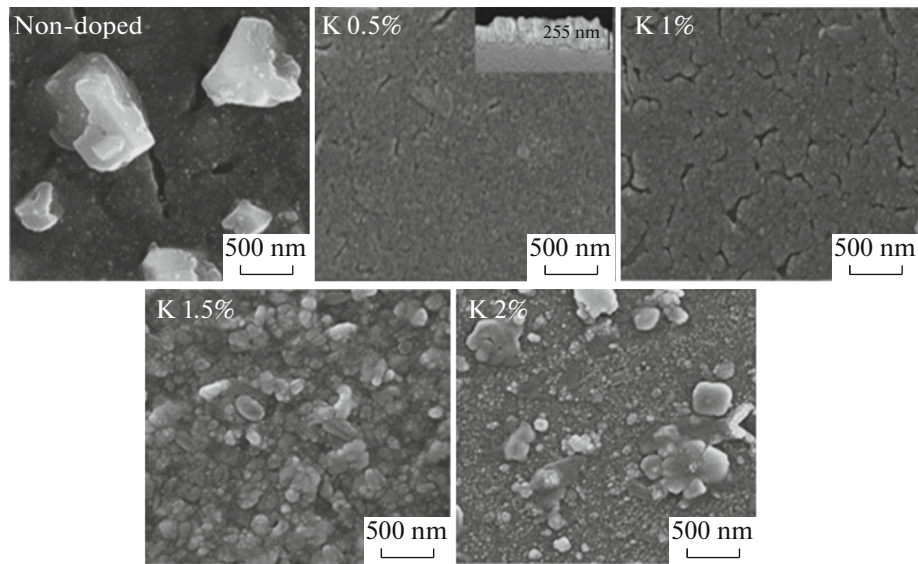


Fig. 4. SEM images for potassium-doped and non-doped CZTS thin films with cross-sectional image inset for K: 0.5% sample.

dopants can be passive and reduce the number of defects in the CZTS lattice with the Cu sites' occupation and reduce the Zn–Cu defects [32].

Other optical constants for the samples such as the refractive indices n and extinction coefficient k can be calculated using α , T , and R , as follows:

$$R = \frac{(n-1)^2 + k^2}{(n+1)^2 + k^2}, \quad (8)$$

$$k = \alpha\lambda/4\pi. \quad (9)$$

The variation in n and k versus energy for the studied samples are shown in Figs. 9 and 10.

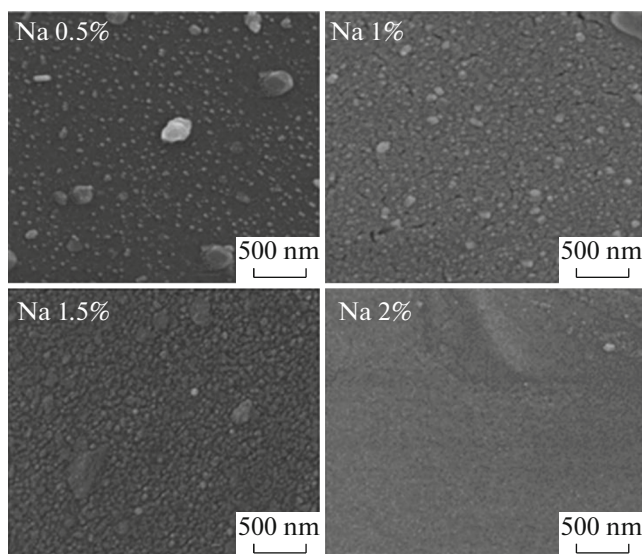


Fig. 5. SEM images for Sodium-doped CZTS thin films.

As shown in Figs. 9 and 10, the samples' refractive index and extinction coefficient vary with the dopant concentration. The refractive index decrease near the absorption edge shows a normal dispersion in the samples. The values of $n(\lambda)$ for the Na-doped samples are in the range of about 1.16–3.9 and 1.13–2.28 at low and high energy region, respectively and for the K-doped samples are in the range of about 1.20–3.78 at both energy region which is in agreement with the values reported in the other works [33, 34]. The $n(\lambda)$ values for the non-doped sample are in the range of about 3.70–2.10 in the measurement energy region. The refractive index's behavior for 1.5% K and 1% Na samples is mostly similar to $n(\lambda)$ for the non-doped sample. The values of $n(\lambda)$ at all measurement energy regions for 1% Na/K sample are higher/lower than the non-doped sample's refractive index. The extinction coefficient behavior is consistent with the absorption spectra (Figs. 7a and 7b). A small refractive index can be due to the successive internal reflections, and dispersion occurs at the boundaries of grains, which happens in 1% K-doping and 0.5% Na-doping, consistent with the structural and morphological results. When the dielectric functions are known, they may be used to study the samples' optical properties. The real ϵ_r and imaginary ϵ_i parts of the dielectric function that show light scattering and absorption within the sample, respectively, are defined as

$$\epsilon_r = n^2 - k^2, \quad (10)$$

$$\epsilon_i = 2nk. \quad (11)$$

The variation in the real and imaginary values for the dielectric functions with energy in Figs. 11a and 11b for K-doped and Figs. 12a–12c for Na-doped samples are shown.

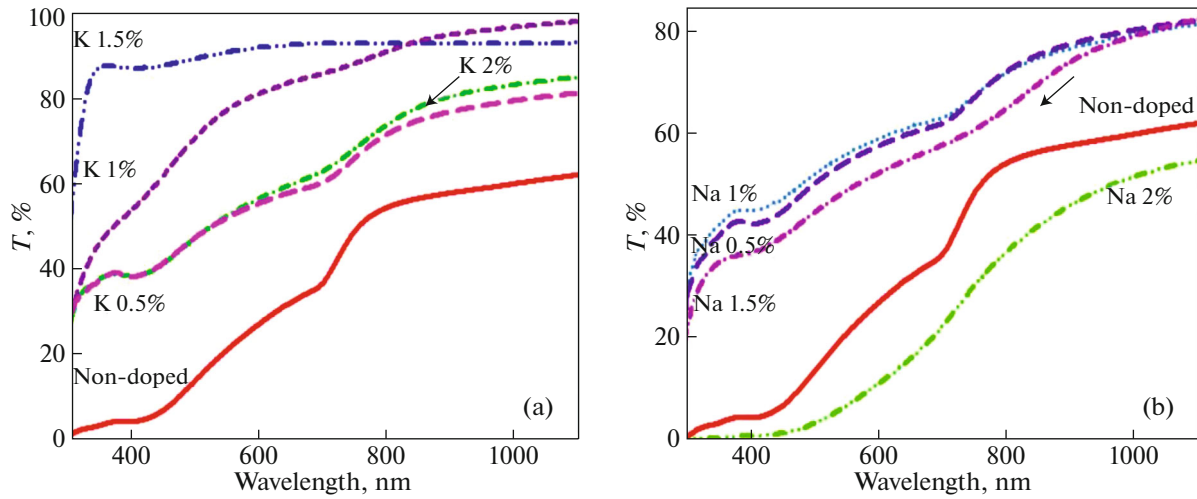


Fig. 6. Transmission spectra of the studied CZTS samples doped with different (a) K concentrations and (b) Na concentrations.

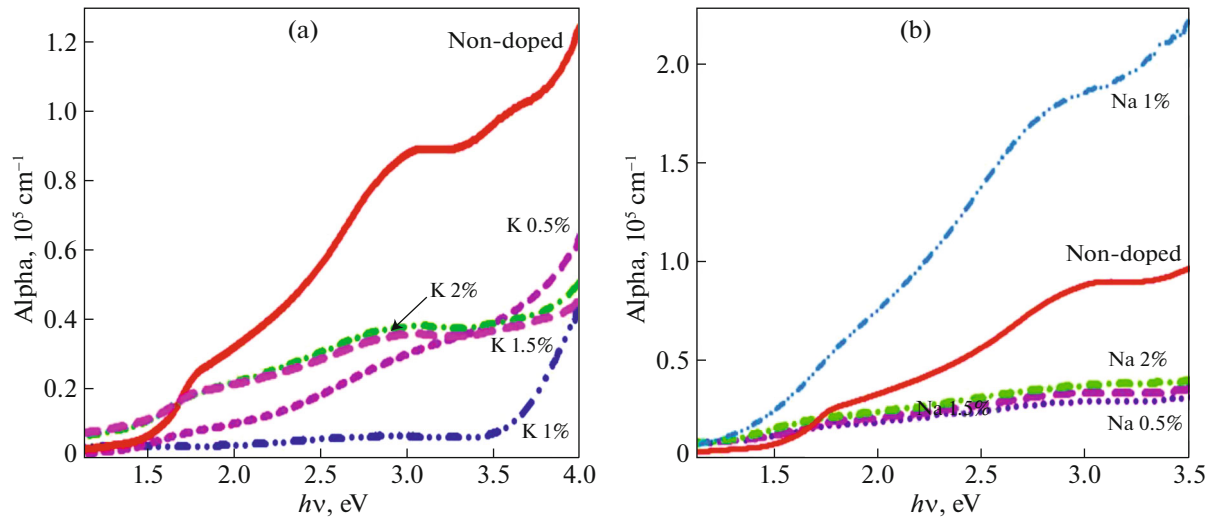


Fig. 7. Absorption coefficient α vs. photon energy $h\nu$ for doped CZTS films with (a) K and (b) Na.

Optical conductivity is a measurement of the sample response to the light. The following equation can obtain the energy dependence of optical conductivity:

$$\sigma_{opt} = anc/4\pi, \tag{12}$$

where c is the speed of light in the vacuum. The variation in the optical conductivity of the CZTS thin films is shown in Fig. 13.

3.3. Electrical Properties

To measure the $I(V)$ curves for the samples, gold contacts were deposited by sputtering on the corner of CZTS thin films. The $I(V)$ characteristics of the samples were measured, and the results obtained were shown in Fig. 14.

All the $I(V)$ curves show linear behaviors with different slopes. Among the K-doped samples, K (1.5%) has the least electrical resistance and K (0.5%) has the highest electrical resistance, and all the doped samples have a lower resistance to the non-doped sample, and among the Na-doped samples, the sample Na (1%) has the least electrical resistance, and the sample Na

Table 5. Values for the optical band gap of K- and Na-doped CZTS thin films

K/Cu ratio, %	0	0.5	1	1.5	2
E_g , eV (K)	1.55	1.59	1.57	1.53	1.50
Na/Cu ratio, %	0	0.5	1	1.5	2
E_g , eV (Na)	1.55	1.46	1.61	1.48	1.40

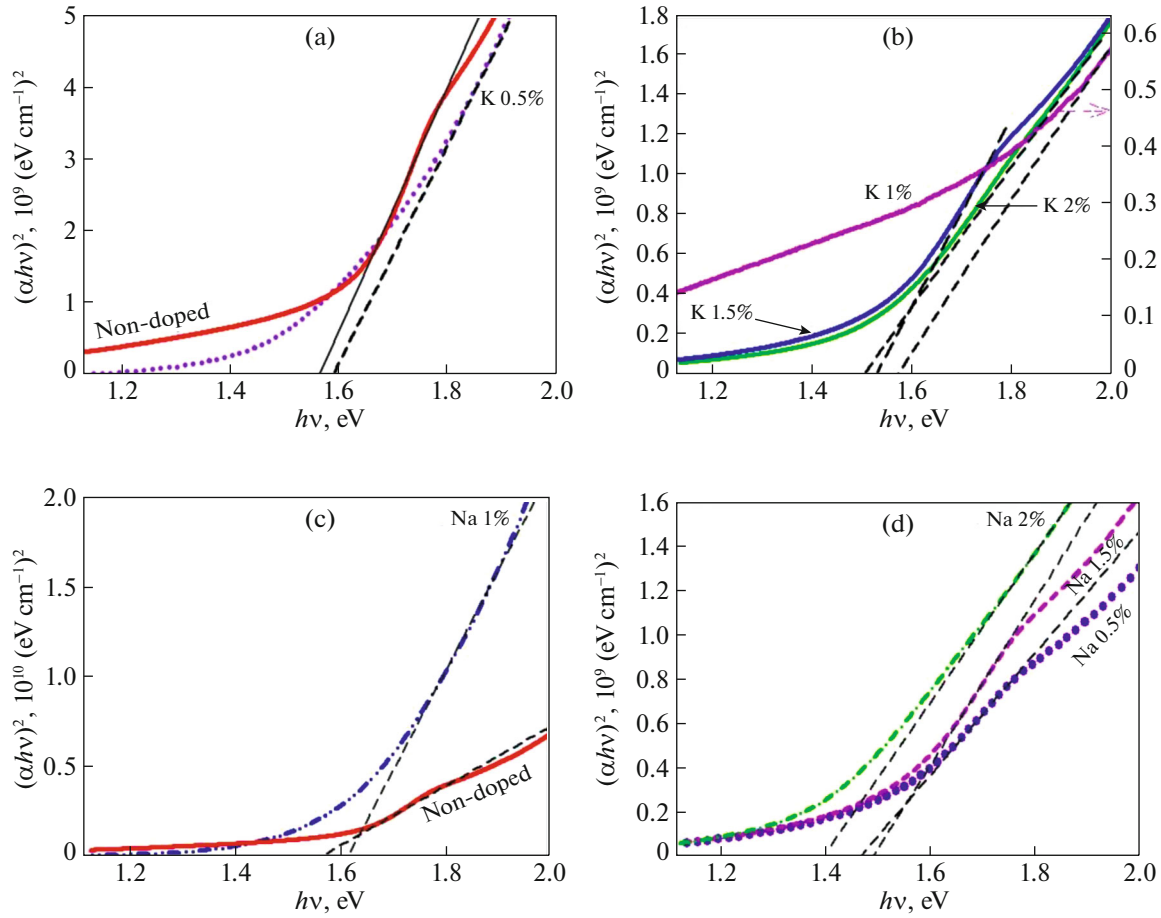


Fig. 8. $(\alpha hv)^2$ vs. photon energy hv of non-doped and doped samples with K (a and b) and Na (c and d) for the calculation of direct band energies.

(2%) has the highest electrical resistance. Moreover, 0.5% Na sample has lower resistance, and 1.5 and 2% Na samples have a higher resistance to the non-doped sample. The CZTS thin film's electrical property is crucial for its performance in photovoltaic devices. The Hall measurements were employed at room temperature to study the electrical properties of the CZTS thin films. The relation between the Hall voltage V_H , applied magnetic field B , and electrical current I is as follows:

$$V_H = \frac{IB}{ned}, \quad (13)$$

where d is the film's thicknesses, n is the carrier concentration, and e is the elementary charge. The Hall coefficient R_H and Hall mobility μ of the samples were calculated using Equations (14) and (15), respectively:

$$R_H = \frac{1}{ne}, \quad (14)$$

$$\mu = \frac{R_H}{\rho}. \quad (15)$$

The resistivity of the samples ρ was determined using the four-probe method. The electrical characteristics of the CZTS thin films are summarized in Table 6.

The Hall measurements indicated that all doped samples were *p-type* semiconductors, and doping up to these levels did not change the type of the carrier of thin films. In the K-doped samples, the charge carrier concentration increases after the doping and resistivity of samples decreases. The carrier concentration increases from $6.15 \times 10^{+18}$ to $8.22 \times 10^{+19} \text{ cm}^{-3}$ as K concentration increases from 0 to 1.5%, and after that, with a further increase in K concentration, the carrier concentration decreases. This decrease can be attributed to the production of carrier traps. After K doping, the mobility of CZTS thin films are decreased except for 1.5% K doping thin film; this may be due to the decrease in the crystallite size and increase in grain boundary scattering, but in 1.5% K doping, the larger grain size caused the lower grain boundary related to the barriers that affect the mobility of the sample.

For the Na-doped samples, the carrier concentration increased from $6.15 \times 10^{+18}$ to $7.28 \times 10^{+18}$ as

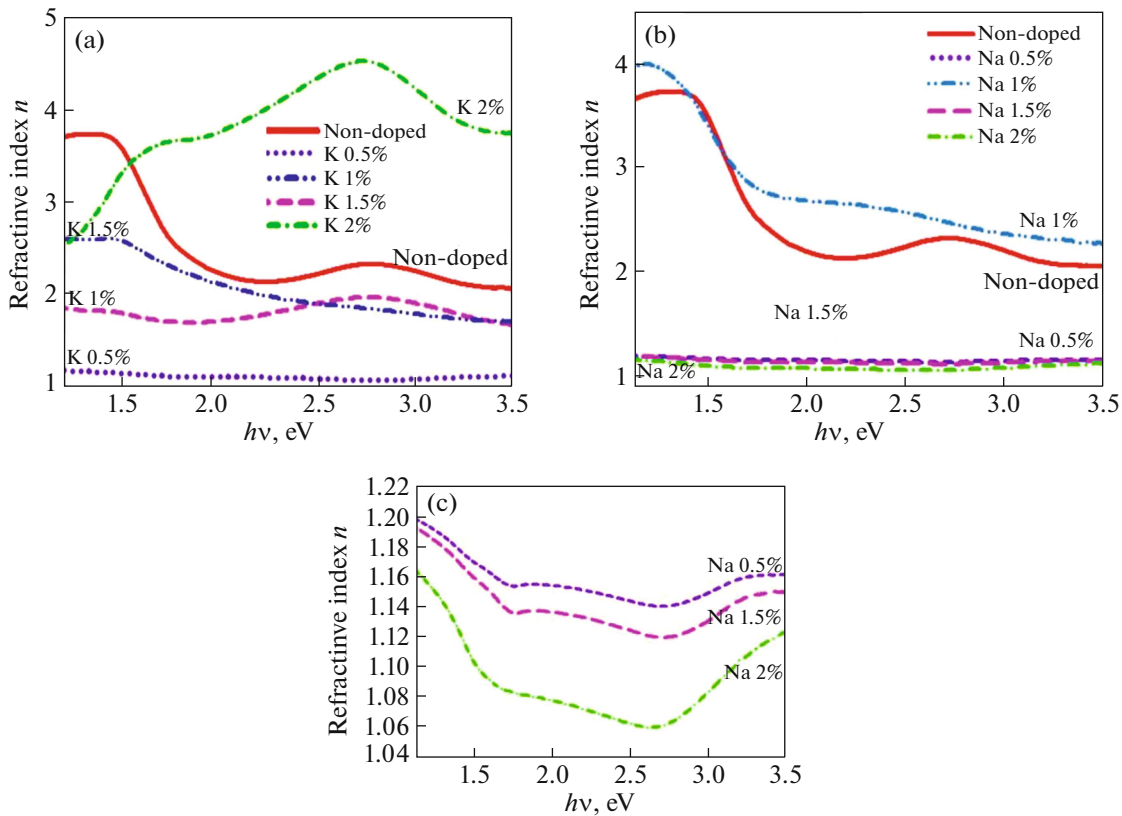


Fig. 9. Refractive index n for CZTS thin films doped with (a) K and (b) Na, (c) to view more detail for Na (0.5, 1.5, and 2%).

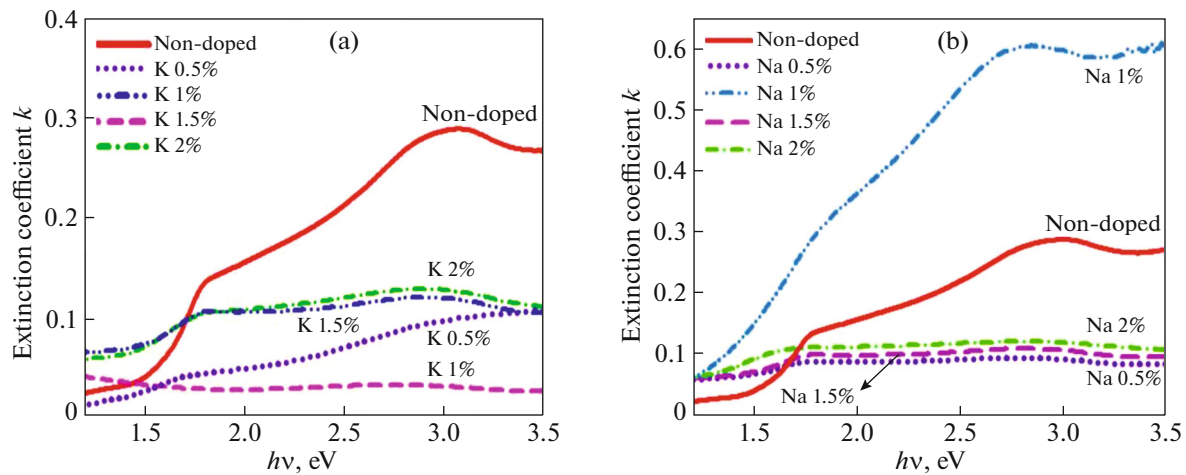


Fig. 10. Extinction coefficient (k) for CZTS thin films doped with (a) K and (b) Na.

K concentration increased from 0 to 1.5% and then decreased again, which is likely to be due to the poor crystallinity, as observed in the Raman measurements (Fig. 3). Na-doped CZTS samples' mobility increases despite the 2% doped sample with minimum grain size. The 1.5% K-doped and 1% Na-doped samples have the lowest resistivity among the samples, which

may be due to the improvement of the crystal structure (larger crystallite sizes), and reduction of the defects in grain boundaries, thereby, decrease the recombination.

Since the CZTS thin films are good candidates for solar cell applications, the samples' photo-electrical

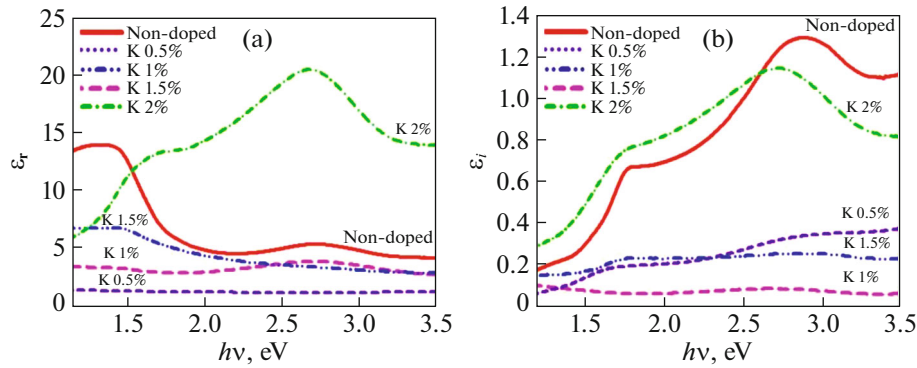


Fig. 11. Variation in the (a) real and (b) imaginary parts of the dielectric constant of K-doped CZTS thin films as a function of photon energy.

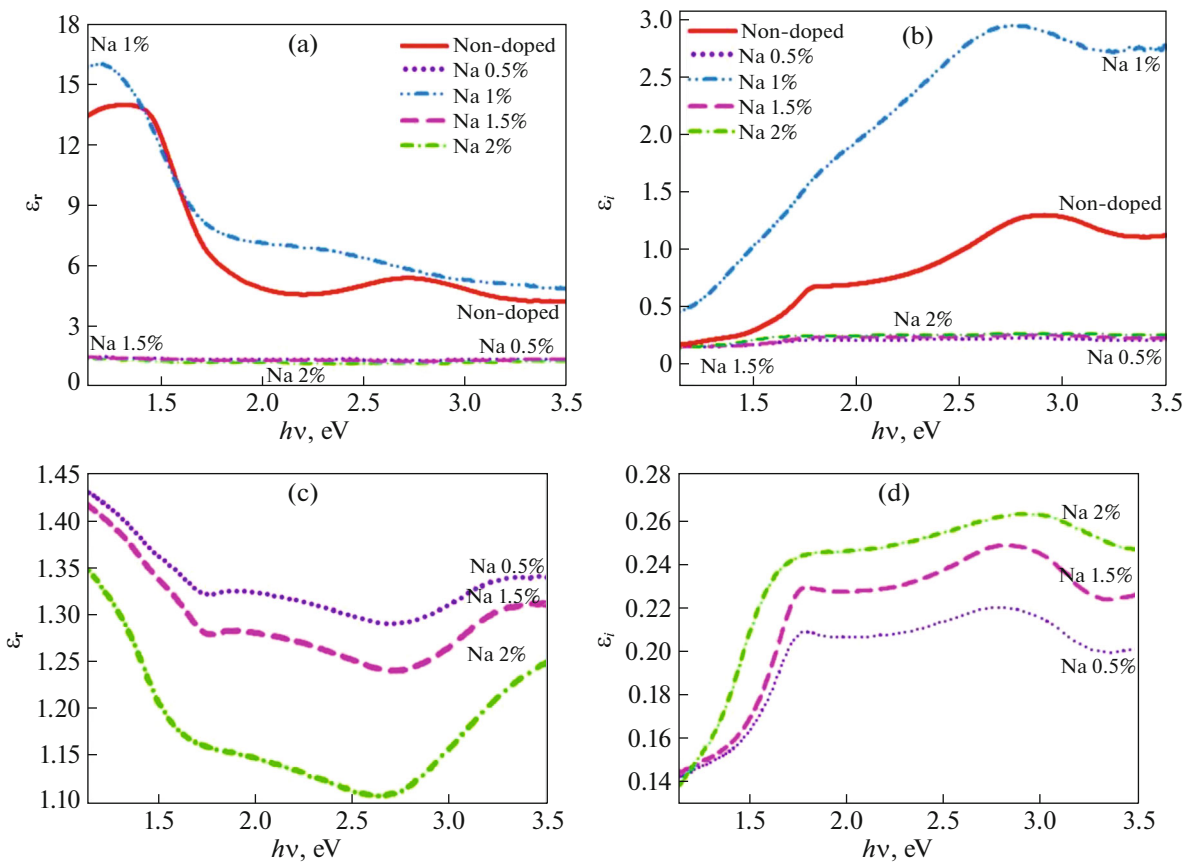


Fig. 12. Variations in the real (a and c) and imaginary (b and d) parts of the dielectric constant of Na-doped CZTS thin films as a function of photon energy; (c) and (d) are added to view more details.

behavior was investigated in the dark and under AM 1.5 (100 mW/cm²) illumination at room temperature. The results obtained are presented in Table 7.

The plot of 1.5% K-doping and 1% Na-doping under illumination and in the dark are shown in Fig. 15.

As we can see, the resistivity of all samples under illumination becomes smaller than that under dark.

This behavior is due to the excitement of charge carriers in the CZTS thin films by the light. The results obtained show a significant increase in the photocurrent under illumination (especially for Na-doped CZTS thin films), indicating that the CZTS thin films are suitable for solar energy conversion. The I_{light}/I_{dark} ratio for the samples doped with 1.5% K and 1% Na doping is 1.74 and 1.61, respectively, which indicates a

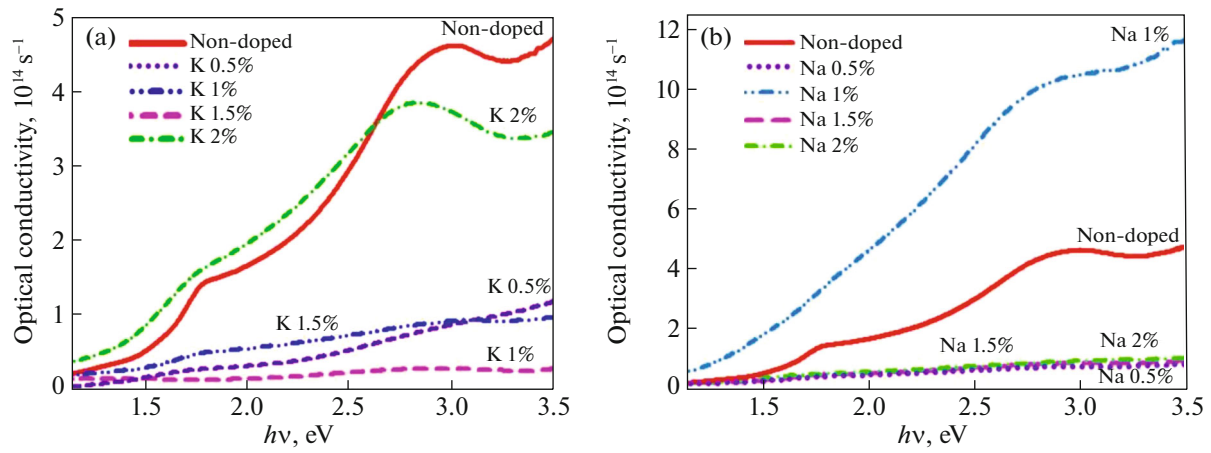


Fig. 13. Variation in optical conductivity of non-doped and doped samples with (a) K and (b) Na doped vs. photon energy $h\nu$.

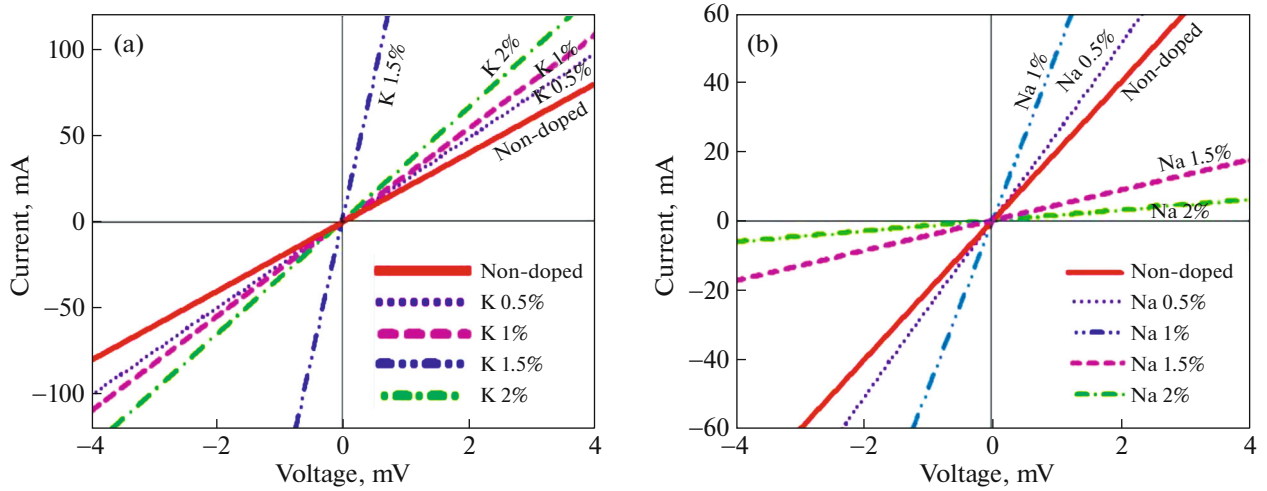


Fig. 14. Measured $I(V)$ curves for non-doped and doped CZTS samples with (a) K and (b) Na.

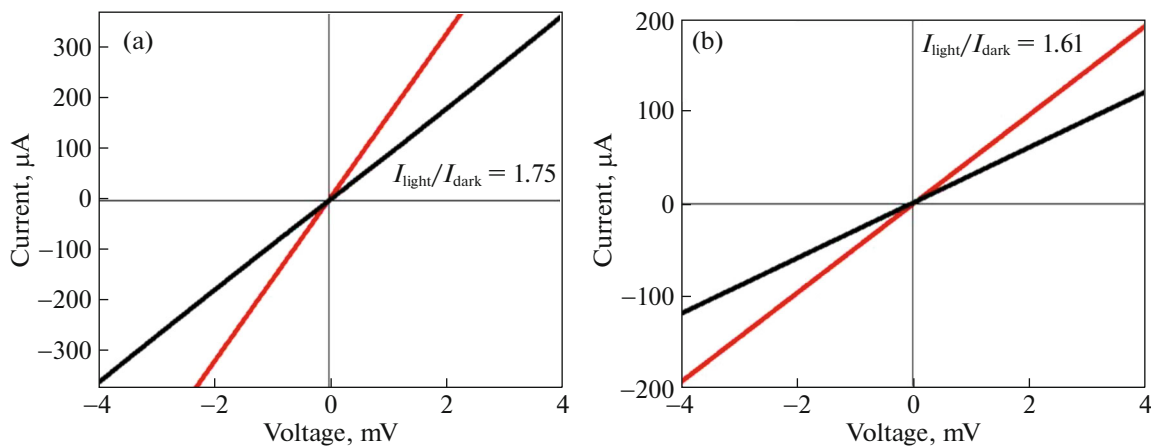


Fig. 15. Current vs. voltage curves and their photocurrent light response for CZTS thin films doped with (a) 1.5% K and (b) 1% Na under irradiation and dark condition.

Table 6. Carrier concentration, Hall coefficient, Hall mobility, and resistivity of CZTS thin films doped with K and Na

K/Cu, %	0	0.5	1	1.5	2
n, cm^{-3}	$6.15 \times 10^{+18}$	$1.85 \times 10^{+19}$	$2.13 \times 10^{+19}$	$8.22 \times 10^{+19}$	$1.04 \times 10^{+19}$
$R_H, \text{cm}^3/\text{C}$	1.015	0.339	0.293	0.076	0.602
$\rho, \Omega \text{ cm}$	10.018	8.213	7.011	0.603	6.375
$\mu, \text{cm}^2/(\text{V s})$	0.101	0.041	0.042	0.126	0.094
Na/Cu, %	0	0.5	1	1.5	2
n, cm^{-3}	$6.15 \times 10^{+18}$	$7.84 \times 10^{+18}$	$1.24 \times 10^{+19}$	$7.28 \times 10^{+18}$	$6.07 \times 10^{+18}$
$R_H, \text{cm}^3/\text{C}$	1.015	0.797	0.504	0.858	1.025
$\rho, \Omega \text{ cm}$	10.019	6.963	4.314	10.418	10.988
$\mu, \text{cm}^2/(\text{V s})$	0.101	0.114	0.117	0.102	0.937

good response to light, and thus the ability of photocurrent producing in CZTS thin films.

To do a detailed study of the doping effects on the photovoltaic device quality of the prepared absorber films, the CZTS|ZnS hetero-junction diodes were fabricated. The structure of the device was a glass|Mo|CZTS|ZnS|Au top electrode. Molybdenum (Mo ~500 nm) was deposited on the glass substrate by the magnetron sputtering method to create an Ohmic back-contact with the CZTS absorber. The CZTS thin film was grown by a sol-gel spin-coated method over the Mo layer, and after that annealed at 500°C with thicknesses of around 1 μm followed by the ZnS (~50 nm) n -type layer deposited by a thermal evaporation method. Then the Au top contacts were deposited by a magnetron sputtering method with a 4.5 mm² area. The current-voltage $I(V)$ characteristics of the p - n CZTS-based diodes of the undoped, 1% Na doping, and 1.5% K-doping samples were measured in the dark and under illumination (AM 1.5, 100 mW/cm²). Figure 16a shows the $I(V)$ characteristics of these CZTS|ZnS devices under illumination.

The results indicated that all devices exhibited a rectifying effect that showed the hetero-junction formed by a p - n junction between CZTS and ZnS.

Table 7. The $I_{\text{light}}/I_{\text{dark}}$ ratio for the CZTS thin films doped with K and Na

K/Cu, %	0	0.5	1	1.5	2
$I_{\text{light}}/I_{\text{dark}}$	1.40	1.21	1.11	1.75	1.16
Na/Cu, %	0	0.5	1	1.5	2
$I_{\text{light}}/I_{\text{dark}}$	1.40	1.49	1.61	1.46	1.36

The fill factor (FF) is a figure of merit of the p - n diodes, which indicates the junction quality of a diode compared to an ideal diode FF that is equal to unity and is defined as the ratio of maximum power ($P_{\text{MP}} = I_{\text{MP}} \cdot V_{\text{MP}}$) produced by a diode to produce V_{oc} and the short-circuit current I_{sc} :

$$\text{FF} = \frac{I_{\text{MP}}V_{\text{MP}}}{I_{\text{sc}}V_{\text{oc}}}, \quad (16)$$

where I_{MP} and V_{MP} are the maximum current and voltage at the $I(V)$ curve, in which the diode has its maximum power output. The detailed device parameters of these samples are summarized in Table 8.

The calculated FF of the diode constructed on CZTS doped with 1.5% K was 0.39, which was more significant than others, but this small value indicated extensive parasitic resistive losses in the junction. The forward current dependence on the applied voltage can be represented by an ideal diode equation:

$$I = I_S \left[\exp\left(\frac{qV}{nkT}\right) - 1 \right], \quad (17)$$

where I_S is the reverse saturation current, q is the electronic charge, V is the applied voltage, n is the diode quality factor, k is the Boltzmann's constant, and T is the absolute temperature. The following relation gives the saturation current:

$$I_S = AA^*T^2 \exp\left(\frac{-q\Phi_b}{kT}\right). \quad (18)$$

In this equation, A is the effective diode area, A^* (63.6A cm⁻² K⁻²) is the effective Richardson constant for CZTS, and Φ_b is the potential barrier height over the carrier thermionic emission. To calculate the

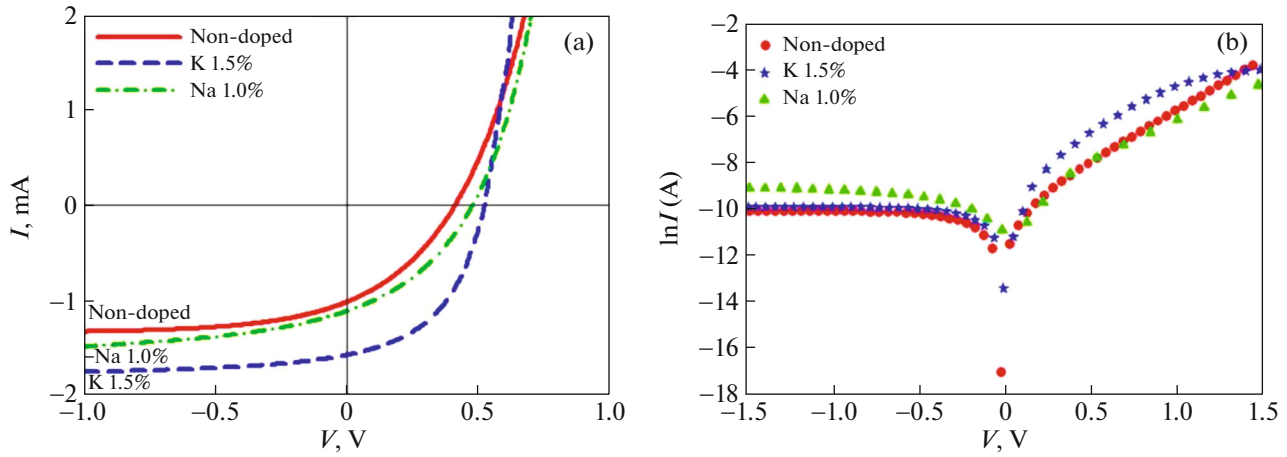


Fig. 16. (a) The light $I(V)$ characteristics and (b) semi-log $I(V)$ plots in the dark for Au|ZnS|CZTS|Mo|glass device for different dopants.

ideality factor, the saturation current, and the barrier height, the dark $I(V)$ characteristic of the non-doped, 1% Na-doping, and 1.5% K-doping samples were plotted on a semi-logarithmic scale, as shown in Fig. 16b. A high value of ideality factor (1 for an ideal $p-n$ diode) may be due to the presence of inter-diffusion, the interfacial layer, the trap-assisted tunneling, the carrier leakage, and the recombination centers such as bulk defects in p -CZTS and grain boundaries [24, 35, 36]. It is important to determine the parasitic resistance of diodes such as series resistance R_s due to the resistance of contacts and the bulk semiconductor and shunt resistance R_{sh} due to shorts or leakage in useless point contacts of semiconductor electrodes. The series resistance and shunt resistance can be calculated by evaluating the dV/dI at high forward and reverse voltages, respectively. The values obtained for the saturation current I_s , ideality factor n , potential barrier height Φ_b , series resistance R_s , and shunt resistance R_{sh} are reported in Table 8.

The measured data indicated that after doping the CZTS thin films, its diode properties were enhanced, and CZTS thin films with 1.5% K-doping had the best performance. The increase in open-circuit voltage and short-circuit current may be due to the grain growth and an increase in the charge carriers. The decreases in the barrier height can be attributed to the improve-

ment in the crystallinity of absorber thin film and formation of proper contact between metal and semiconductor, and the improvement in the ideality factor indicates a decrease in the recombination centers in the CZTS thin film and a reduction in the carrier leakage.

CONCLUSIONS

In this work, we studied the effects of the doping concentration (K/Cu and Na/Cu: 0.5, 1, 1.5, 2%) on the structural, optical, and electrical properties of the CZTS thin films (with an average thickness of 250 nm) deposited by a spin-coating sol-gel method on a glass substrate. The structural study (XRD and Raman analyses) showed that all samples had a kesterite structure, and the microscopic strain, crystallite size, and lattice parameter change with changing the doping concentration and an appropriate amount of dopants can improve them. By the way, in the XRD pattern of some samples (0.5% K, 0.5 and 1.5% Na), some small diffraction peaks related to Cu_{2-x}S , secondary phase was observed. The SEM images and Raman analysis showed that the samples' surface and crystalline quality significantly improve with an appropriate amount of dopants (1% Na and 1.5% K). The optical study showed that introducing K and Na (except 2% Na) to

Table 8. Diode parameters of the CZTS thin films doped with K and Na

Dopant ratio, %	V_{oc} , V	I_{sc} , mA	FF	I_s , A	Φ_b , eV	n	R_s , Ω	R_{sh} , $k\Omega$
0	0.43	1.01	0.35	2.73×10^{-5}	0.59	8.28	45	252
K/Cu (1.5%)	0.53	1.58	0.39	3.06×10^{-6}	0.40	1.99	40	678
Na/Cu (1%)	0.48	1.12	0.36	1.18×10^{-5}	0.42	5.73	41	460

the CZTS system increases the transmittance compare to the non-doped sample. Although the absorption coefficients for all K sample and Na (0.5, 1.5, 2%) samples were smaller than a non-doped sample, for 1% Na layer the absorption coefficients in the visible range were significantly higher (up to $1.8 \times 10^5 \text{ cm}^{-1}$) than non-doped layers, which is an interesting result for the photovoltaic application. The K and Na samples' band gap values were in the range of 1.50–1.59 eV and 1.40–1.61 eV, respectively. Hence, the band gap values had a higher variance for Na-doped samples (about 10%) than the band gap of the non-doped sample (1.55 eV). The behavior of refractive index for 1.5% K and 1% Na samples was mostly similar to $n(\lambda)$ for a non-doped sample, and their values in all measurement energy region for 1% Na/K sample was higher/lower than the refractive index of the non-doped sample. The extinction coefficient behavior of the samples was consistent with their absorption spectra. This work also showed that the prepared CZTS thin films had a good optical conductivity (10^{12} – 10^{15} S^{-1}). The variation in the real and imaginary values for the dielectric functions with energy was in agreement with the other optical parameters. Investigation of the CZTS thin films' electrical properties showed that the carrier concentration significantly increased up to $8.00 \times 10^{19} \text{ cm}^{-3}$ (one order of magnitude increase) with the doping. The results of the Hall measurements indicated that all doped samples were *p*-type, and doping up to these levels did not change the type of the thin films character. The photo-electrical study of the samples showed that for all samples, photocurrent under illumination significantly increased (especially for Na-doped CZTS thin films), indicating that the CZTS thin films are suitable for solar energy conversion. Indeed, the results of this work showed that the CZTS thin films doped with 1.5% K-doping and 1% Na-doping had better properties and with a controllable doping level could reach the most improved properties of the CZTS absorber layer for a solar cell device. Moreover, the results showed that the fabricated (1.5% K or 1% Na)-doped CZTS-ZnS hetero-junction exhibited good rectifying behavior than a non-doped sample and that the doped layers had better diode parameters.

FUNDING

The Shahrood University of Technology provided funding.

CONFLICTS OF INTERESTS

The authors declare that they have no conflict of interest.

REFERENCES

1. N. Nakayama and K. Ito, *Appl. Surf. Sci.* **92**, 171 (1996).
2. J. Kim, H. Hiroi, T. K. Todorov, O. Gunawan, M. Kuwahara, T. Gokmen, D. Nair, M. Hopstaken, B. Shin, Y. S. Lee, W. Wang, H. Sugimoto, and D. B. Mitzi, *Adv. Mater.* **26**, 7426 (2014).
3. P. Jackson, D. Hariskos, E. Lotter, S. Patel, R. Wuerz, R. Menner, W. Wischmann, and M. Powalla, *Prog. Photovolt. Res. Appl.* **19**, 894 (2011).
4. First Solar, Press Release. <http://investor.firstsolar.com>. Accessed December 19, 2015.
5. W. Shockley and J. H. Queisser, *J. Appl. Phys.* **32**, 510 (1961).
6. R. Caballero, C. A. Kaufmann, T. Eisenbarth, T. Unold, S. Schorr, R. Hesse, R. Klenk, and H.-W. Schock, *Phys. Status Solidi A* **206**, 1049 (2009).
7. P. S. Vasekar and N. G. Dhere, *Sol. Energy Mater. Sol. Cells* **93**, 69 (2009).
8. H. Xin, S. M. Vorpahl, A. D. Collard, I. L. Braly, A. R. Uhl, B. W. Krueger, D. S. Ginger, and H. W. Hillhouse, *Phys. Chem. Chem. Phys.* **17**, 23859 (2015).
9. J. V. Li, D. Kuciauskas, M. R. Young, and I. L. Repins, *J. Appl. Phys. Lett.* **102**, 163905 (2013).
10. Z. Tong, C. Yan, Z. Su, F. Zeng, J. Yang, Y. Li, L. Jiang, Y. Lai, and F. Liu, *J. Appl. Phys. Lett.* **105**, 223903 (2014).
11. D. Tiwari, T. Koehler, X. Lin, R. Harniman, I. Griffiths, L. Wang, D. Cherns, R. Klenk, and D. J. Fermin, *Chem. Mater.* **28**, 4991 (2016).
12. B. Shin, O. Gunawan, Y. Zhu, N. A. Bojarczuk, S. J. Chey, and S. Guha, *Prog. Photovolt.: Res. Appl.* **21**, 72 (2013).
13. D. Nam, S. Cho, J.-H. Sim, K.-J. Yang, D.-H. Son, D.-H. Kim, J.-K. Kang, M.-S. Kwon, C.-W. Jeon, and H. Cheong, *Sol. Energy Mater. Sol. Cells* **149**, 226 (2016).
14. Y. B. Kishore Kumar, P. Uday Bhaskar, G. Suresh Babu, and V. Sundara Raja, *Phys. Status Solidi A* **207**, 149 (2010).
15. R. D'Angelo, C. L. A. Azanza Ricardo, A. Mittiga, P. Scardi, and M. Leoni, *J. Sol-Gel Sci. Technol.* **72**, 490 (2014).
16. C. Kim and S. Hong, *Mol. Cryst. Liq. Cryst.* **645**, 217 (2017).
17. K. Tanaka, N. Moritake, and H. Uchiki, *Sol. Energy Mater. Sol. Cells* **91**, 1199 (2007).
18. R. Hosseinpour, M. Izadifard, M. E. Ghazi, and B. Bahramian, *J. Electron. Mater.* **47**, 1080 (2018).
19. P. Scherrer, *Göttinger Nachr. Math. Phys.* **2**, 98 (1918).
20. G. K. Williamson and W. H. Hall, *Acta Metall.* **1**, 22 (1953).
21. Y. Xia, Z. Chen, Z. Zhang, X. Fang, and G. Liang, *Nanoscale Res. Lett.* **9**, 208 (2014).
22. Z. Seboui, A. Gassoumi, and N. Kamoun-Turki, *Mater. Sci. Semicond. Process.* **26**, 360 (2014).

23. A. Martinez-Ayala, M. Pal, N. R. Mathews, and X. Mathew, *Can. J. Phys.* **92**, 875 (2014).
24. P. A. Fernandes, P. M. P. Salomé, and A. F. da Cunha, *J. Alloys Compd.* **509**, 7600 (2011).
25. K. Wang, B. Shin, K. B. Reuter, T. Todorov, D. B. Mitzi, and S. Guha, *J. Appl. Phys. Lett.* **98**, 051912 (2011).
26. Y. Zhao, W. Tao, X. Chen, J. Liu, and A. Wei, *J. Mater. Sci.: Mater. Electron.* **26**, 5645 (2015).
27. K. Diwate, K. Mohite, M. Shinde, S. Rondiya, A. Pawbake, A. Date, H. Pathan, and S. Jadkar, *Energy Proc.* **110**, 180 (2017).
28. J. Tauc, R. Grigorovici, and A. Vancu, *Phys. Status Solidi B* **15**, 627 (1966).
29. S. M. Pawar, B. S. Pawar, A. V. Moholkar, D. S. Choi, J. H. Yun, J. H. Moon, S. S. Kolekar, and J. H. Kim, *Electrochim. Acta* **55**, 4057 (2010).
30. K. Tanaka, M. Oonuki, N. Moritake, and H. Uchiki, *Sol. Energy Mater. Sol. Cells* **93**, 583 (2009).
31. Z. Y. Zhao and X. Zhao, *Inorg. Chem.* **53**, 9235 (2014).
32. W. Xiao, J. N. Wang, X. S. Zhao, J. W. Wang, G. J. Huang, L. Cheng, L. J. Jiang, and L. G. Wang, *Sol. Energy* **116**, 125 (2015).
33. B. U. Maheshwari and V. S. Kumar, *Int. J. Energy Res.* **39**, 771 (2015).
34. G. Yang, Y. F. Li, B. Yao, Z. H. Ding, R. Deng, X. Fang, and Z. P. Wei, *ACS Appl. Mater. Interfaces* **7**, 16653 (2015).
35. R. Qin, H. Cao, L. Liang, Y. Xie, Z. Fei, H. Zhang, J. Gao, K. Javaid, C. Liu, and W. Z. Sun, *Appl. Phys. Lett.* **108**, 142104 (2016).
36. F. Z. Boutebakh, M. Lamri Zeggar, N. Attaf, and M. S. Aida, *Optik* **144**, 180 (2017).